Rietveld refinements of the paraelectric and ferroelectric structures of $PbFe_{0.5}Ta_{0.5}O_3$

2000 J. Phys.: Condens. Matter 12 2367

(http://iopscience.iop.org/0953-8984/12/11/303)

J. Phys.: Condens. Matter **12** (2000) 2367–2378. Printed in the UK PII: S0953-8984(00)08925-6

Rietveld refinements of the paraelectric and ferroelectric structures of $PbFe_{0.5}Ta_{0.5}O_3$

Nathascia Lampis†, Philippe Sciau‡§ and Alessandra Geddo Lehmann†

† Dipartimento di Fisica e INFM, Cittadella Universitaria, Strada Provinciale Monserrato-Sestu Km 0.700, 09042 Monserrato (CA), Italy

‡ CEMES-CNRS, 29 rue Jeanne Marvig, BP 4347, 31055 Toulouse Cédex, France

Received 25 October 1999

Abstract. The high symmetry parent phase and the two derived low symmetry phases of the complex perovskite $PbFe_{0.5}Ta_{0.5}O_3$ have been refined by the Rietveld method from neutron powder diffraction data. The analysed powders were obtained by grinding single crystals. Owing to the very small distortions from the cubic structure, the lattice symmetry of the derived phases was determined by means of synchrotron radiation powder diffraction. At 350 K the cubic phase (which is known to be stable for $T > 270$ K) is characterized by positional disorder or anharmonic thermal motion of lead atoms, as happens in most Pb-based complex perovskites. It was refined in space group $Pm\bar{3}m$, with strongly anisotropic thermal motion of oxygen atoms. The synchrotron powder diffraction pattern of the intermediate phase (stable for 220 K $< T <$ 270 K), collected at 230 K, agrees with a small tetragonal distortion. Neutron data at 230 K were refined in symmetry $P4mm$. Only oxygen atoms are significantly displaced from the cubic positions. The analysis of line broadening and splitting in the synchrotron radiation patterns collected at 130 K and 15 K indicate the low temperature symmetry to be monoclinic. Neutron data at 15 K were refined in space group Cm.

1. Introduction

$PbFe_{0.5}Ta_{0.5}O_3$ is a compound belonging to the family of Pb-based complex perovskites with general formula $PbB'_xB''_{1-x}O_3$. It was first synthesized as a ceramic by Smolenskii *et al* in 1959 [1] who discovered also its ferroelectricity. Materials of this kind typically undergo a sequence of temperature-induced ferroic phase transitions, which, from the structural point of view, consist in small distortions of a highly symmetric parent phase or *prototype*. From this ideally undistorted phase, all the less symmetric *ettotypes* are derived.

The sequence of phases one finds in Landolt–Börnstein [2] is at first sight quite simple, indicating one slightly diffuse transition from a cubic prototype, of space group $Pm\bar{3}m$, to a rhombohedral derived phase of symmetry $R3m$ [3, 4]. A Curie range of about 40 K around $T_C = 243$ K was indicated. However, this simple scenario has become more complicated since single crystals were synthesized. Different studies led us to hypothesize the presence of a double phase transition and to question the rhombohedral symmetry of the low temperature phase [5, 6]. In the most recent study performed on single crystals [7] the existence of the second transition was confirmed by high resolution x-ray diffraction and polarized light microscopy. The two transition temperatures define the stability range of three phases: a cubic high symmetry phase ($T > T_{c1} = 270$ K), a tetragonal intermediate phase (220 K $> T >$ 270 K) and a low temperature monoclinic one ($T < T_{c2} = 220$ K). In this paper the refinements

§ Author to whom all correspondence should be addressed.

0953-8984/00/112367+12$30.00

of the three structures of $PbFe_{0.5}Ta_{0.5}O_3$ are presented and discussed. With this aim, powder diffraction data have been collected at different temperatures, chosen on the basis of the results of [7]. Because of the very weak lattice distortions present in the less symmetric phases, the lattice symmetry has been determined at each temperature from synchrotron radiation data. In contrast, for the best location of oxygen atoms and the correct determination of thermal parameters, structure refinements have been performed from neutron diffraction data.

Powder techniques have been preferred in order to avoid problems posed by the presence of ferroelastic domains below the first phase transition. However, owing to the difficulties offered by the synthesis of $PbFe_{0.5}Ta_{0.5}O_3$ ceramics, in order to achieve consistency with the results determined in our previous works, carried out on single crystals, the herewith analysed powders were obtained by grinding crystals grown under the same conditions as described in [10] and used in [5–7]. The same choice was recently made in studying the analogous compound $PbFe_{0.5}Nb_{0.5}O_3$, for which an intermediate tetragonal phase has been observed only in single crystals [8] and for which the low temperature structure has been definitely refined in monoclinic symmetry [8, 9] from diffraction data obtained for powdered single crystals. Actually, discrepancies between results obtained for crystals and for ceramics are frequent in the field of complex perovskites and must be ascribed to the complexity of the phenomena associated with the synthesis of this class of compounds. As mentioned, the preparation of ceramics of $PbFe_{0.5}Ta_{0.5}O_3$ and $PbFe_{0.5}Nb_{0.5}O_3$ by direct reaction of precursor oxides presents major difficulties due to the high stability of a competing iron-deficient pyrochlore phase with composition $Pb_2Fe_{2x}Ta(Nb)_{2-x}O_{7+x/2}$. As a result, a two-phase product is invariably obtained, with relative phase content strongly dependent on the choice of the thermal treatment temperatures. The high volatility of PbO easily produces Pb off-stoichiometry and further pyrochlore stabilization. In the case of $PbFe_{0.5}Ta_{0.5}O_3$ the alternative procedure known as the wolframite route, consisting in the preparation of the intermediate compound $FeTaO_4$ and in its subsequent reaction with PbO to give the final perovskite, does not solve the problem. According to our experience, elimination of pyrochlore can be achieved by preliminary prolonged high energy milling of starting oxides. Unfortunately, iron contamination is one of the most common and almost inevitable effects of ball milling, and it is difficult to say to what extent such impurities can influence the fine balance between competing phases which differ just for slight distortions. The growth of single crystals of $PbFe_{0.5}Ta_{0.5}O_3$ presents minor difficulties. Crystals can be grown from a high temperature flux of PbO, which avoids contamination. The Pb-rich liquid ambient minimizes Pb off-stoichiometry. If the growth is correctly performed (i.e. is carried out under equilibrium conditions), crystals are well faceted, cube shaped and can be easily separated from the secondary pyrochlore, which has different colour and morphology (octahedral habit).

2. Experimental procedure

2.1. Samples

Details on single crystal growth conditions have been reported in [10]. Residual PbO flux was removed by washing crystals in hot 30% nitric acid. Pyrochlore crystals were separated by hand under the polarized light microscope. Crystals of $PbFe_{0.5}Ta_{0.5}O_3$ to be ground to powder were carefully chosen to be free from PbO inclusions. To relax residual strain possibly caused by grinding, the obtained powder was annealed for several hours at $T = 850$ K, a procedure already adopted in the study of mechanically polished single crystal sections [7]. The final perovskite powder was subjected to preliminary x-ray diffraction, which proved it to be very well crystallized, with sharp Bragg reflections, and free from the secondary phase.

2.2. Data collection and refinement

The neutron experiments were performed at the Laboratoire Léon Brillouin† using the Orphée reactor facilities (Saclay, France) on a thermal source. Powder diffraction patterns were collected on the high resolution two-axis goniometer 3T2 ($\lambda = 1.225$ Å), equipped with a cryofurnace, using steps of 0.05° between 6 and 125° (2θ), $\sin\theta_{max}/\lambda = 0.72$ Å^{-1}. The measuring temperatures were chosen as 520 K, 230 K and 15 K, with a temperature stability of 0.5 K.

Synchrotron radiation data were collected on the beam line BM 16 of the European Synchrotron Radiation Facility (ESRF) at Grenoble. The powder was sealed in a 0.3 mm diameter capillary and, to minimize the absorption, a wavelength of 0.412 28 Å was used. Data were collected using an Si(111) monochromator and the detector consisted of a Ge(111) nine-channel multi-analyser stage with a separation of two degrees between each channel. Diffractograms were recorded at 520 K and 350 K using a stream of hot air and at 230 K, 130 K and 15 K in the cryostat ($\sin\theta_{max}/\lambda = 0.95$ Å^{-1}).

Structure refinements were carried out using the profile Rietveld method by means of the program XND [11]. Experimental details are given in table 1.

Table 1. Measurements and refinement conditions of neutron data.

Data collection	
Diffractometer	3T2 (LLB)
Monochromator	Ge(115)
Instrument geometry	Transmission
Temperature (K)	350, 230, 15
Wavelength (Å)	1.225
Step (2θ); range (2θ)	0.05°; 6–125°
$(\sin\theta)/\lambda_{max}$ (Å^{-1})	0.72
Number of points	2380
Refinements	
Refinement on	$S = \sum w_i(Y_{0i} - Y_{ci})^2$
Weighting scheme	$w_i = 1/Y_{0i}$
Analytical function for profile	Pseudo-Voigt
R-factors	$R_{wp} = \left\{\left(\sum w_i(Y_{0i} - Y_{ci})^2\right)\left(\sum w_i(Y_{0i})^2\right)^{-1}\right\}^{1/2}$
	$R_B = \left(\sum \lvert I_{0k} - I_{ck}\rvert\right)\left(\sum I_{0k}\right)^{-1}$
	GoF $= [S/(N-P)]^{1/2}$
	R_{wp_c} = modified R_{wp} taking into account the local correlation [12]
Program for refinement	XND 1.12 [11]

3. Results

3.1. Synchrotron radiation data

3.1.1. Symmetries of the low temperature phases. In a first step, all the collected diffraction patterns were compared. No splitting of reflections is observed in the passage from cubic to intermediate phase ($T = 270$ K). However, while hhh reflections are not modified in size (figures 1 and 3), the $h00$ are enlarged as shown in figures 2 and 3. This result is consistent with the very weak tetragonal distortion proposed for the intermediate phase [7]. Below 220 K

† Laboratoire commun CEA–CNRS.

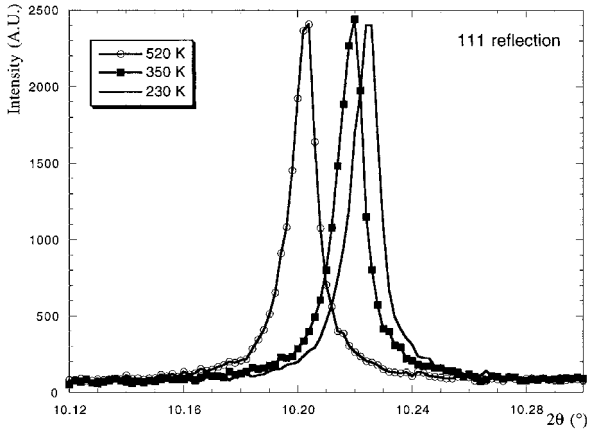

Figure 1. 111 Reflections at 520, 350 and 230 K.

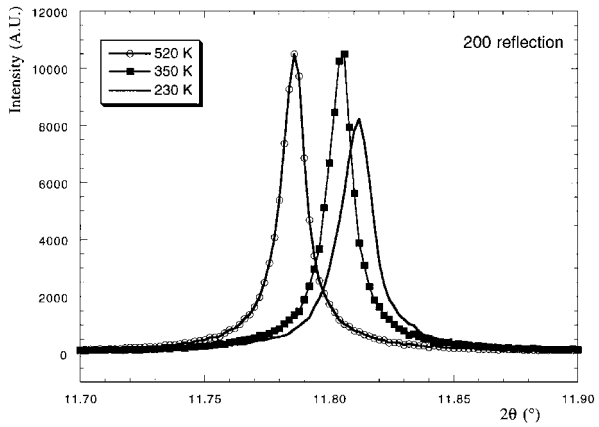

Figure 2. 200 Reflections at 520, 350 and 230 K.

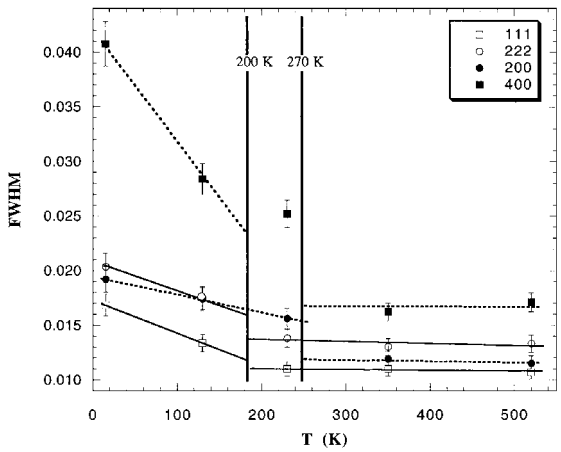

Figure 3. Full width at half maximum (FWHM) of reflections versus temperature.

Table 2. Cell parameters from the ESRF data ($a_m = (a_c + b_c)/2$, $b_m = (-a_c + b_c)/2$ and $c_m = c_c$).

T (K)	a (Å)	b (Å)	c (Å)	β (°)
520	4.0162(1)			
350	4.0097(1)			
230	4.0069(2)		4.0087(2)	
130	5.6696(4)	5.6623(4)	4.0086(3)	89.886(5)
15	5.6687(4)	5.6610(4)	4.0083(2)	89.853(4)

the hhh reflections are well split, while the enlargement of $h00$ reflections still increases (figure 3). In [7] it was shown that the splitting of the 400 reflection increases while lowering temperature. Unfortunately, the instrumental resolution of our experiment was not adequate for direct observation of $h00$ splitting. However, the observed enlargements agree well with the monoclinic symmetry proposed for the low temperature phase. In addition to the enlargements of $h00$ reflections, a small enlargement of all reflections is observed at the lowest temperatures.

In a second step, we determined the cell parameters according to the phase sequence proposed in the study on single crystal [7]. A profile matching, with the Rietveld method, was performed in the cubic space group $Pm\bar{3}m$, on data at 520 K and 350 K. With the same fixed profile parameters, the data at 230 K were refined in the tetragonal $P4mm$ symmetry. At 130 K and 15 K the cubic profile parameters were only used as starting point for the refinement in the monoclinic symmetry Cm. Results are reported in table 2. The values of the cell parameters are in good agreement with the interplanar distances given in [7].

3.1.2. Analysis of the $|F(hkl)|$ versus $\sin\theta/\lambda$. An analysis of the behaviour of the modulus of the structure factor $|F(hkl)|$ as a function of $\sin\theta/\lambda$ has been performed to make some considerations about the behaviour of Pb atoms in $PbFe_{0.5}Ta_{0.5}O_3$. In the ideal cubic perovskites (ABO_3), Bragg reflections can be broken down into four types, following the parity of Miller indices, i.e. $(odd, odd, even)$, $(even, even, even)$, (odd, odd, odd) and $(odd, even, even)$. In the general case, $|F(hkl)|$ versus $\sin\theta/\lambda$ should be a monotonically decreasing function for the four types of reflection. However, $|F(odd, odd, odd)|$ and $|F(odd, even, even)|$ can present a minimum, as already observed in the cubic phases of $PbMg_{1/3}Nb_{2/3}O_3$ [13, 14] and $PbSc_{0.5}Ta_{0.5}O_3$ [14]. Such a kind of behaviour has been ascribed either to static disorder of Pb or to a strong anharmonic thermal motion of this atom.

The experimental $|F_e(hkl)|$ versus $\sin\theta/\lambda$ for the four types of reflection of $PbFe_{0.5}Ta_{0.5}O_3$ at 350 K is shown in figure 4. The curves of $|F_e(odd, odd, even)|$ and $|F_e(even, even, even)|$ behave as expected (figure 4(b)). The curves of $|F_e(odd, odd, odd)|$ and $|F_e(odd, even, even)|$ present a minimum (figure 4(a)). In order to verify if the non-monotonic behaviour can be reproduced by a harmonic model, $|F(\sin\theta/\lambda)|$ has been calculated and compared to the experimental curves. With this aim, atoms were located in special positions of the cubic perovskite structure with the isotropic thermal factors $B(\mathrm{Pb}) = 3.5$ Å^2, $B(\mathrm{Fe/Ta}) = 0.5$ Å^2 and $B(\mathrm{O}) = 1$ Å^2 obtained from refinements of neutron data (cf section 3.2.1, table 3, model a and table 4). Results are displayed in figure 4(a). It can be seen that the experimental curves are very well reproduced up to $\sin\theta/\lambda \cong 0.7$ Å^{-1}. However, beyond this value the experimental points lie above the calculated curves, which is especially true for the (odd, odd, odd) reflections. As the non-monotonic behaviour of $|F(\sin\theta/\lambda)|$ is due to the large difference between the atomic thermal motions of Pb and Fe/Ta, this result indicates that a simple harmonic, non-disordered structural model is not completely adequate for describing the cubic phase of $PbFe_{0.5}Ta_{0.5}O_3$.

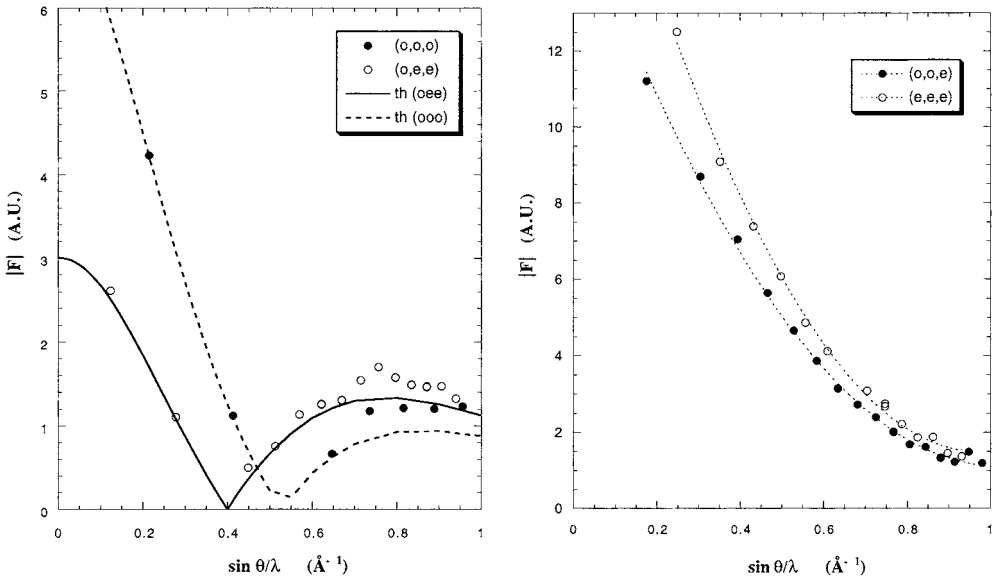

Figure 4. $|F(hkl)|$ versus $\sin\theta/\lambda$ at 350 K. The continuous curves correspond to the theoretic evolution in the ideal model (atoms in cubic special positions, $B(\mathrm{Pb}) = 3.5$ Å^2, $B(\mathrm{Fe/Ta}) = 0.5$ Å^2 and $B(\mathrm{O}) = 1$ Å^2).

Table 3. R-factors of the neutron data refinement at 350 K: (a) all atoms in the special positions, (b) Pb shifted along the ⟨100⟩ directions, (c) Pb shifted along the ⟨110⟩ directions.

	R_{wp} (%)	R_{wpc} (%)	R_B (%)	GoF	Δ(Pb) (Å)	B(Pb)	No of structural parameters
a	4.39	7.68	2.39	1.33		3.5 (1)	7
b	4.31	7.22	2.22	1.31	0.257 (6)	1.6 (1)	8
c	4.27	7.11	2.09	1.30	0.283 (5)	1.1 (1)	8

Table 4. Structural parameters at 350 K. Space group $Pm\bar{3}m$, model c. $B_{eq} = (4/3)\sum\sum\beta_{ij}\vec{a}_i\vec{a}_j$.

Atom	x	y	z	B_{eq} (Å^2)	β_{11}	β_{22}	β_{33}
Fe/Ta in 1b	0.5	0.5	0.5	0.50(1)			
Pb in 12i	0.0499(9)	0.0499(9)	0	1.1(1)			
O in 3c	0.5	0.5	0	1.05	0.0212(3)	0.0212(3)	0.0057(4)

We have been tempted to perform the same analysis on the intermediate phase. Since the tetragonal distortion is very weak and no splitting of reflections is observed, we have considered that an analysis of the structure factor $|F_e(hkl)|$ versus $\sin\theta/\lambda$ could be performed in the cubic approximation. Figure 5 shows the evolution of $|F_e(odd, even, even)|$ at three temperatures. There is a weak difference between the curves in the cubic phases (520 and 350 K) and in the intermediary one (230 K) but, as the compared patterns were not collected under the same conditions, it is advisable to be careful in evaluation. However, it is clear that the 'anomalous' behaviour of Pb does not present a significant evolution through the phase transition (270 K).

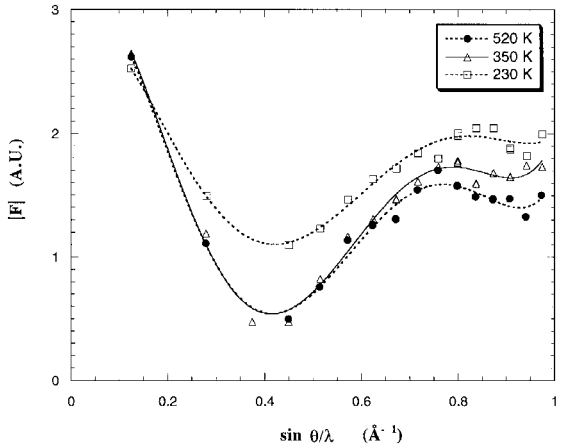

Figure 5. The dependence of $|F(hkl)|$ on $\sin\theta/\lambda$ at 520 K, 350 K and 230 K. The curves are just guidelines for the eye.

3.2. Rietveld refinements of neutron data

The cell parameters were fixed on the values given in table 2. The wavelength and the profile parameters were refined in the cubic phase at 350 K. The obtained values were used for the refinement at 230 and 15 K.

3.2.1. Phase at 350 K. The structure was refined in cubic space group $Pm\bar{3}m$ with all atoms in special positions and in the harmonic approximation for thermal motions. As typical for the Pb-based perovskites, the Debye–Waller factor for Pb is abnormally large (displacement parameter $B_{Pb} = 3.5$ Å^2). Although a Pb deficiency appears unlikely because of the preparation method, nevertheless at this point the Pb stoichiometry was tested by refining the Pb occupancy factor. The refined value indicated full site occupancy with an unchanged value of B_{Pb}. Therefore the meaning of such a large Pb displacement parameter has been examined. This point has been widely discussed in the literature [9]. It is known that improvements can be obtained considering Pb located in a multi-minimum potential around its Wyckoff position. We have tested the three possible kinds of Pb disorder usually considered, i.e.: along ⟨100⟩, ⟨110⟩ and ⟨111⟩ directions. Both the ⟨100⟩ and ⟨110⟩ models lead to a weak fall of R-factors (table 3). The difference between these two models is not so pronounced as for the similar compound $PbFe_{0.5}Nb_{0.5}O_3$ [9]. The Pb shift is also smaller. It has been noted [13] that a set of high symmetry directions for Pb displacements can appear to be preferred with respect to the others just as a consequence of a too small value of the maximum measured $\sin\theta/\lambda$. However, as $PbFe_{0.5}Ta_{0.5}O_3$ neutron data were collected under the same conditions as $PbFe_{0.5}Nb_{0.5}O_3$, the absence of anisotropy in Pb shifts seems to be significant. It has been suggested that an anharmonic treatment of the thermal motion of Pb should be better adapted [15] in this case, but with this aim it would be necessary to have data up to a $\sin\theta/\lambda$ value greater than our neutron data. A refinement of synchrotron data in anharmonic approximation is in progress [15]. In any case, it is clear that the cubic phase of $PbFe_{0.5}Ta_{0.5}O_3$ presents the same characteristic as other cubic complex Pb-based perovskites and that a non-disordered model with a Pb harmonic thermal motion is not satisfactory. As for other perovskites, the thermal ellipsoid of the oxygen atom is strongly anisotropic. The final structural parameters of the actual best model are given in table 4.

Table 5. Results of refinement at 230 K. Models: C1 ($Pm\bar{3}m$): ordered, all thermal motions isotropic. T1 ($P4mm$): ordered, all thermal motions isotropic. T2 ($P4mm$): ordered, anisotropic thermal motions for Pb and O.

	R_{wp} (%)	R_{wp_c} (%)	R_B (%)	GoF	No of parameters
Model C1	5.80	14.9	5.24	1.78	27
Model T1	5.07	11.8	2.88	1.56	29
Model T2	4.82	10.7	2.41	1.49	35

Table 6. Final structural parameters at 230 K ($R_{wp} = 4.82\%$, $R_B = 2.41\%$). Space group $P4mm$. Oxygen thermal displacements are mainly perpendicular to the Fe/Ta–O bonds. $B_{eq} = 4/3 \sum\sum \beta_{ij}\vec{a}_i\vec{a}_j$.

Atom	x	y	z	B_{eq} (Å^2)	β_{11}	β_{22}	β_{33}
Fe/Ta in 1b	0.5	0.5	0.5	0.41(6)			
Pb in 1a	0	0	−0.021(3)	3.34	0.053(3)	0.053(3)	0.050(5)
O1 in 1b	0.5	0.5	0.016(6)	0.59	0.011(4)	0.011(4)	0.006(6)
O2 in 2c	0.5	0	0.475(3)	0.93	0.015(5)	0.005(2)	0.023(4)

3.2.2. Intermediate phase at 230 K. The intermediate phase was refined in the tetragonal space group $P4mm$ as for the intermediate phase of the perovskite $PbFe_{0.5}Nb_{0.5}O_3$ [9]. The cubic model of symmetry $Pm\bar{3}m$ was also tested for comparison.

In a first step, atomic thermal motions were chosen isotropic (models T1 and C1, respectively for tetragonal and cubic). For the two symmetries the Debye–Waller factors of Pb were abnormally large (3.64(1) Å^2 and 3.54(3) Å^2 respectively). A better agreement was obtained with model T1 (cf table 5), confirming the tetragonal symmetry.

In a second step, both Pb and O were refined anisotropically (model T2). This led to a further improvement in the R-factors (cf table 5). The thermal ellipsoids of oxygen atoms are strongly anisotropic, leading to vibrations occurring mainly perpendicular to the O–Fe/Ta bonds, as in the cubic phase. In contrast, the thermal ellipsoid of Pb is very close to a sphere with an equivalent thermal factor $B_{eq} = 3.54$ Å^2 comparable to the isotropic one of the cubic phase before the introduction of positional disorder. There is not an heavy modification of Pb disorder at the cubic/tetragonal phase transition in agreement with the analysis of the structure factor $|F(hkl)|$ presented in section 3.1.2 (figure 5). The structural parameters for the tetragonal structure (model T2) are reported in table 6.

3.2.3. Low temperature phase at 15 K. Neutron data of the low temperature phase was refined in the monoclinic space group Cm as for $PbFe_{0.5}Nb_{0.5}O_3$ [9]. The rhombohedral model of space group $R3m$ was also used for comparison.

For the two models, the cubic positions were used as initial ones. We used isotropic thermal factors for O and Fe/Ta, while Pb was treated anisotropically. The monoclinic model gives the best result, as shown in table 7. The Rietveld refinement of the neutron pattern in monoclinic symmetry is shown in figure 6 and the structural parameters are given in table 8.

The thermal ellipsoid of Pb is found to be large and strongly anisotropic. This point, widely discussed for $PbFe_{0.5}Nb_{0.5}O_3$ [9] (that presents the same characteristic in the monoclinic phase), indicates that Pb is still disordered at 15 K. The atomic displacements in the monoclinic and rhombohedral models are very similar. The main distortion is rhombohedral and the structure can be considered as pseudo-rhombohedral in first approximation. The thermal

Table 7. Results of refinement at 15 K.

	R_{wp} (%)	R_{wp_c} (%)	R_B (%)	GoF	No of parameters
Monoclinic model	4.82	10.54	2.74	1.50	36
Rhombohedral model	4.99	11.78	3.00	1.55	30

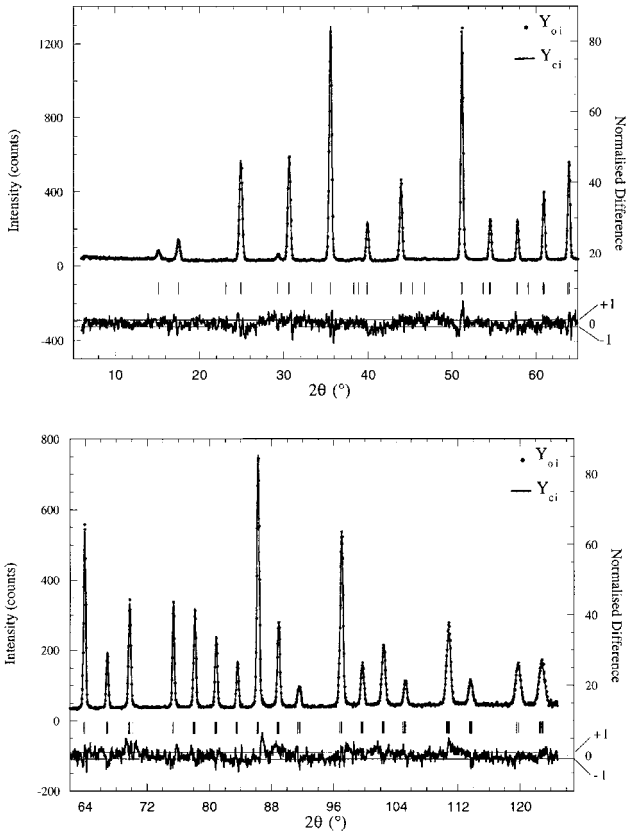

Figure 6. Rietveld refinement of neutron diffraction pattern at $T = 15$ K, showing the experimental and the calculated profile. The normalized difference curve $\Delta_{norm} = (Y_{0i} - Y_{ci})/\sigma(Y_{0i})$ is plotted at the bottom. Lines corresponding to $\Delta_{norm} = \pm 1$ are indicated.

ellipsoid is flattened along the pseudo-ternary axis ($U_1 = 0.0085$ Å^2) and spread in the normal plane ($U_2 = 0.032$ Å^2, $U_3 = 0.053$ Å^2).

4. Discussion

The present structural study has confirmed that $PbFe_{0.5}Ta_{0.5}O_3$ is isostructural with $PbFe_{0.5}Nb_{0.5}O_3$. The two compounds have the same sequence of phases, the structures of which are isotypical, as can be seen by comparing the structural parameters (tables 4, 6 and 8) and the bond lengths (table 9), reported in this paper, with the equivalent results (tables 2, 4, 7 and 8) of [9].

In the intermediate phase of $PbFe_{0.5}Ta_{0.5}O_3$ the tetragonal strain is largely smaller than in $PbFe_{0.5}Nb_{0.5}O_3$ ($c/a = 1.0004(1)$ instead of 1.0015(5)), which explains why for the

Table 8. Final structural parameters for the monoclinic model at 15 K. Space group Cm.

Atom	x	y	z	B_{eq} (Å^2)	β_{11}	β_{22}	β_{33}	β_{33}
Fe/Ta	0.5	0	0.5	0.34(4)				
Pb	0.022(4)	0	0.021(5)	2.42	0.014(3)	0.020(3)	0.048(7)	−0.018(4)
O1	0.513(3)	0	0.010(4)	0.4(1)				
O2	0.236(2)	0.241(2)	0.470(2)	0.4(1)				

Table 9. Bond lengths (Å) at 350 K, 230 K and 15 K obtained from neutron refinements. In the cubic phase the disorder of Pb and O atoms was not considered.

Distance	Cubic	Tetragonal	Monoclinic
Fe/Ta–O	2.005(1) × 6	1.94(3) × 1	1.97(2) × 1
		2.006(1) × 4	1.99(1) × 2
		2.07(3) × 1	2.03(1) × 2
			2.05(2) × 1
Pb–O	2.835(1) × 12	2.82(1) × 4	2.57(2) × 2
		2.837(1) × 4	2.78(3) × 1
		2.85(1) × 4	2.83(2) × 2
			2.831(1) × 2
			2.86(2) × 2
			2.89(3) × 1
			3.11(3) × 2
O–O	2.835(1) × 12	2.72(2) × 4	2.68(2) × 1
		2.833(1) × 4	2.73(3) × 2
		2.95(2) × 4	2.78(2) × 2
			2.842(1) × 2
			2.90(2) × 2
			2.93(3) × 2
			3.01(2) × 1

herewith studied compound it was not possible, even with synchrotron resolution, to observe the splitting of $h00$ reflections. The distortions and the ferroelectric shifts of the two Fe-containing compounds are very small (table 10) if compared to those of the related perovskite $PbTiO_3$ [16]. It has been remarked that in $PbTiO_3$ the marked shift of Pb along one pseudo-cubic $\langle 100 \rangle$ direction allows the formation, with the four nearest oxygen atoms located at a distance of 2.52 Å, of PbO_4 coordination polyhedra, which would be at the origin of the high stability of this tetragonal phase [17]. As can be seen from table 9, in tetragonal $PbFe_{0.5}Ta_{0.5}O_3$ the minimum Pb–O distance attains the value of 2.82(1) Å, which is only slightly shortened with respect to what is found in the cubic phase. Moreover, Pb conserves, in tetragonal $PbFe_{0.5}Ta_{0.5}O_3$ and $PbFe_{0.5}Nb_{0.5}O_3$, large thermal parameters. It is well known that a conventional diffractometric analysis does not allow us to distinguish between static positional disorder and large dynamic vibrations, as they are both described within the formalism of the Debye–Waller factor. However, one can comment that in the case of static disorder the pseudocubic symmetry of the intermediate phases of $PbFe_{0.5}Ta_{0.5}O_3$ and $PbFe_{0.5}Nb_{0.5}O_3$ should reflect the absence of long range correlations between Pb shifts along the three $\langle 100 \rangle$ directions, as proposed in [18], while in the case of large dynamic vibrations, which should be anharmonic according to the analysis performed in section 3.1.2, the Pb–O hybridization should be absent, which is consistent with the very weak observed tetragonal strain.

It may be interesting to compare $PbFe_{0.5}Ta_{0.5}O_3$ and $PbFe_{0.5}Nb_{0.5}O_3$ with the two relaxor compounds $PbSc_{0.5}Ta_{0.5}O_3$ and $PbSc_{0.5}Nb_{0.5}O_3$. In contrast to what happens in Fe-containing

Table 10. Comparison of the ferroelectric shifts in $PbFe_{1/2}Ta_{1/2}O_3$, $PbFe_{1/2}Nb_{1/2}O_3$ [9], $PbTiO_3$ [16], $PbSc_{1/2}Nb_{1/2}O_3$ (PSN) ordered and disordered [21], $Pb(Mg_{0.3}Nb_{0.6}Ti_{0.1})O_3$ [22] and $BaTiO_3$ [23].

	$PbFe_{1/2}Ta_{1/2}O_3$		$PbFe_{1/2}Nb_{1/2}O_3$		$PbTiO_3$	Dis. PSN	Ord. PSN	PMN-PT	$BaTiO_3$
	P4mm	*Cm*	*P4mm*	*Cm*	*P4mm*	*R3m*	*R3m*	*R3m*	*R3m*
	230 K	15 K	363 K	250 K	295 K	10 K	10 K	90 K	204 K
δ_{A-O} (Å)	0.04(3)	0.22(4)	0.00(3)	0.23(4)	0.49(4)	0.35(5)	0.34(5)	0.29(5)	0.10(5)
δ_{B-O} (Å)	0.05(3)	0.07(5)	0.02(3)	0.10(5)	0.31(5)	0.12(6)	0.10(6)	0.07(6)	0.18(6)

compounds, the degree of long range order on octahedral sites in the two Sc-based perovskites can be modified by suitable thermal treatments, with profound effects on the dielectric properties [19, 20]. Nevertheless, both the ordered and the disordered forms show the same low temperature rhombohedral structure [21]. This structure is very similar to the monoclinic one of $PbFe_{0.5}Ta_{0.5}O_3$ and $PbFe_{0.5}Nb_{0.5}O_3$. They are both characterized by large shifts of Pb atoms along the [111] rhombohedral (or pseudo-rhombohedral) direction. The shift is a bit smaller for the Fe-containing compounds (table 10). The shifts of B-type atoms are also a bit smaller, and comparable to the one observed in $Pb(Mg_{0.3}Nb_{0.6}Ti_{0.1})O_3$ (PMN-PT) [22]. It is remarkable that these structures differ substantially from the rhombohedral structure of $BaTiO_3$ [23]. In contrast to what happens in barium titanate, in fact, the shift of the A-type cation is larger than the shift of the B-type one and the thermal parameter of A (i.e. of Pb) is large and strongly anisotropic. Temperatures are low enough to exclude a dynamic origin of such large thermal parameters, so that in the rhombohedral phases of $PbFe_{0.5}Ta_{0.5}O_3$, $PbFe_{0.5}Nb_{0.5}O_3$, $PbSc_{0.5}Ta_{0.5}O_3$ and $PbSc_{0.5}Nb_{0.5}O_3$ lead atoms can be considered to be statically disordered. From the refined shape of the thermal ellipsoid, the disordered positions are found to be in the plane normal to the [111] rhombohedral axis. Some considerations can be made about this particular Pb configuration. As we have already mentioned [9], Pb-based complex perovskites can be classified according to whether the distortion of their less symmetric phase is orthorhombic or rhombohedral. The latter class includes $PbFe_{0.5}Ta_{0.5}O_3$ and $PbFe_{0.5}Nb_{0.5}O_3$ for which, as stated, the main distortion is rhombohedral in spite of the overall monoclinic symmetry. It is found that in compounds belonging to the first class the thermal ellipsoid of Pb, large at high temperature, attains a normal value in the less symmetric phase. This is the case, for example, of Pb_2MgWO_6 [24], for which $B_{Pb} = 2.83$ Å^2 at 350 K and $B_{Pb} = 0.34$ Å^2 at 80 K. In contrast, in all the known compounds of the second class the thermal ellipsoid of Pb remains abnormally large down to the lowest measured temperatures, and in this sense Pb can be still described by means of split-site models. It has been suggested [18] that one reason for adoption of split positions in the rhombohedrally distorted compounds may be the tendency of Pb to form PbO_4 coordination polyhedra. This structural layout, realized in the orthorhombic phases, is forbidden in rhombohedral symmetry but can be restored, at least locally, if Pb moves away from the ternary axis and splits over several sites around it. In contrast, an ordered configuration with Pb in a special position on the threefold axis would allow only the PbO_3 coordination. Up to now, there is no known example of a Pb-based perovskite in which a coordination of the type PbO_3 is present together with a normal thermal parameter of Pb.

Acknowledgments

The authors are grateful to Dr F Bourée and E Dooryhee for help in neutron and synchrotron experiments, respectively.

References

[1] Smolenskii G A, Agranovskaia A I and Ysupov V A 1959 *Fiz. Tverd. Tela* **1** 990 (in Russian) (Engl. Transl. 1959 *Sov. Phys.–Solid State* **1** 907)
[2] *Landolt–Börnstein New Series* 1990 Group III, vol 28 (Berlin: Springer)
[3] Nomura S, Takabayashi H and Nakagawa T 1968 *Japan. J. Appl. Phys.* **7** 600
[4] Nomura S, Kaneta K and Abe M 1979 *J. Appl. Phys.* **18** 681
[5] Geddo Lehmann A, Kubel F and Schmid H 1997 *J. Phys.: Condens. Matter* **9** 8201
[6] Geddo Lehmann A, Kubel F, Ye Z-G and Schmid H 1995 *Ferroelectrics* **172** 277
[7] Geddo Lehmann A and Sciau Ph 1999 *J. Phys.: Condens. Matter* **11** 1235
[8] Bonny V, Bonin M, Sciau Ph, Schenk K J and Chapuis G 1997 *Solid State Commun.* **102** 347
[9] Lampis N, Sciau Ph and Geddo Lehmann A 1999 *J. Phys.: Condens. Matter* **11** 3489
[10] Brixel W, Boutellier R and Schmid H 1987 *J. Cryst. Growth* **82** 396
[11] Bérar J F and Garnier P 1992 *APD 2nd Conf. (NIST Special Publication 846)* (Washington, DC: US Government Printing Office) p 212
XND is available by anonymous ftp at ftp://labs.polycnrs-gre.fr/pub/xnd
[12] Bérar J F and Lelann P 1991 *J. Appl. Crystallogr.* **24** 1
[13] Vakhrushev S, Zhukov S, Fetisov G and Chernyshov V 1994 *J. Phys.: Condens. Matter* **6** 4021
[14] Zhukov S G, Chernyshev V V, Aslanov L A, Vakhrushev S B and Schenk H 1995 *J. Appl. Crystallogr.* **28** 385
[15] Kiat J M 1999 private communication
[16] Nelmes R J, Piltz R O, Kuhs W F, Tun Z and Restiri R 1990 *Ferroelectrics* **108** 165
[17] Cohen R E 1992 *Nature* **358** 136
[18] Rivezzi N and Sciau Ph 1998 *J. Solid State Chem.* **139** 332
[19] Chu F, Setter N and Tagantsev A K 1993 *J. Appl. Phys.* **74** 5129
[20] Chu F, Reaney I M and Setter N 1995 *J. Appl. Phys.* **77** 1671
[21] Malibert C, Dkhil B, Kiat J M, Durand D, Bérar J F and Spasojevic-de Biré A 1997 *J. Phys.: Condens. Matter* **9** 7485
[22] Noblanc O, Gaucher P and Calvarin G 1996 *J. Appl. Phys.* **79** 4291
[23] Hewat A W 1974 *Ferroelectrics* **6** 215
[24] Baldinozzi G, Sciau Ph, Pinot M and Grebille D 1995 *Acta Crystallogr.* B **51** 668